Correlation Based Phase Noise Compensation in 60 GHz Wireless Systems

Nicholas Preyss, Radoslav D. Pantić, and Andreas Burg
Telecommunications Circuits Laboratory, EPF Lausanne, 1015 Lausanne, Switzerland
e-mail: {nicholas.preyss, radoslav.pantic, andreas.burg}@epfl.ch

***Abstract*—The necessity of phase noise (PN) compensation in future 60 GHz communication systems is shown in this paper. Based on a reference hardware testbed we evaluate the impact of PN on the transmission performance. We show that long data transmissions can only be obtained with PN compensation even for low modulation orders. A low-complexity algorithm for phase noise estimation and compensation based on auto-correlation of pilot words is described. An efficient all-digital architecture for the proposed algorithm is presented.**

I. Introduction

The increasing problem of limited bandwidth and congestion in currently used frequency bands has become a significant limitation for the proliferation of WiFi in recent years. The new standards at 60 GHz offer a considerable increase in available bandwidth, as well as high spatial selectivity compared to established WiFi standards. The resulting boost in capacity enables a greater number of users to be supported and new, exciting applications. For example, wireless streaming of raw HD and 4K video data allows to finally replace cable-based connections for high-resolution video applications.

While research into 60 GHz communication originally has been focused on high throughput in-room links, it is now under consideration for the next generation cellular systems [1][2].

The introduction of 60 GHz communication systems means an increase in bandwidth and carrier frequency by more than an order of magnitude compared to current WiFi system. Such a leap poses challenges for the precision of the analog front-end. It becomes clear that these challenges can not be completely compensated for by improved analog design techniques, but instead, mm-wave baseband receivers will have to put an emphasis on the compensation of hardware impairments, compared to current below-6 GHz communication systems.

A. Outline

The remainder of this paper is structured as follows. In Section II we introduce our setup to evaluate the influence of phase noise on single-carrier system performance and present our simulation results. Section III describes our proposed algorithm for estimation and compensation of phase noise and provides compensation performance results. Considerations regarding a VLSI implementation of the proposed algorithms are given in Section IV. Finally a conclusion is drawn in Section V.

B. System Model

Throughout this paper elements of a vector are set in lower-case with a subscript for the index, if we refer to the vector as a whole it is set without a subscript and in boldface. For constants upper-case letters are used. Hence, a vector of transmitted symbols, of length N_{TX}, is denoted by $\mathbf{s}$ and specific elements by $s_i, i = 0, .., N_{\text{TX}}\text{-}1$.

The effect of frequency selectivity of the transmission channel and analog components is applied in time-domain as inter symbol interference (ISI) in the complex baseband representation. In order to keep notation simple, we model the different sources of ISI as a single channel impulse response (CIR) $\mathbf{h}$ of length N_{CIR}. Further we assume that $\mathbf{h}$ is properly aligned so that it consists purely of taps with a significant contribution to the signal energy and is normalized to unit power.

Phase noise (PN) is described by a vector, $\boldsymbol{\phi}$, of the same length N_{RX} as the vector of received samples $\mathbf{r}$. The elements $r_i, i = 0, .., N_{\text{RX}}\text{-}1$ of $\mathbf{r}$ are therefore defined as,

$$r_i = e^{j2\pi\phi_i} \left(\sum_{k=0}^{N_{\text{CIR}}-1} s_i h_{i-k} \right) + w_i, \tag{1}$$

where w_i are i.i.d. samples of a Gaussian distribution and model the influence of thermal noise. This model implies PN only impacts the RX side of the transmission. This simplification is valid as long as $\phi_i \approx \phi_j, \forall |i-j| < N_{\text{CIR}}$. If this condition is met, the various PN effects can be modeled as a single PN source in the receiver.

We assume the reference frequency offset and as well as the low frequency components of the PN are considered as static frequency offset and are compensated beforehand by a synchronization unit.

The signal-to-noise-ratio (SNR) is used to describe the power of the thermal noise $P_{\mathbf{w}}$ relative to the signal power $P_{\mathbf{s}}$ and is defined as, $\text{SNR} = \frac{P_{\mathbf{s}}}{P_{\mathbf{w}}}$. Total distortion of the received signal is quantified in terms of an error vector magnitude (EVM). In our model distortion in the receiver is caused by the thermal noise power $P_{\mathbf{w}}$ and the PN power P_{PN}, hence EVM is defined

$$\text{EVM} = \sqrt{\frac{P_{\text{PN}} + P_{\mathbf{w}}}{P_{\mathbf{s}}}} \tag{2}$$

$$= \sqrt{\frac{P_{\text{PN}}}{P_{\mathbf{s}}} + \frac{1}{SNR}}. \tag{3}$$

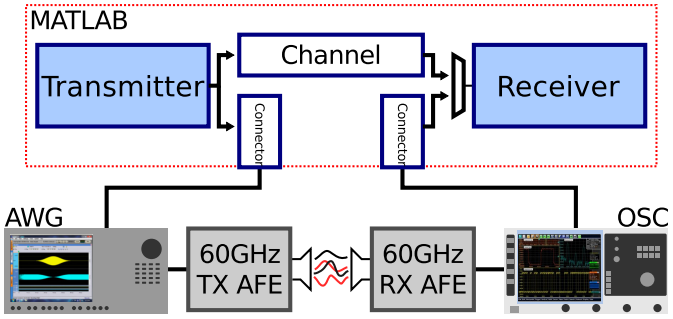

Fig. 1. Integrated MATLAB/hardware simulation approach.

In the absence of PN the entire distortion of the received samples is caused by thermal noise and $\frac{1}{\sqrt{SNR}}$ is the lower bound of the EVM.

II. Impact of Phase Noise on System Performance

In order to evaluate the impact of PN on 60 GHz communication we use a simulation-hardware co-design approach. A 60 GHz hardware testbed is used as a reference for a MATLAB-based simulation framework. This approach assures that the performance simulation is based on sound assumptions.

A. Simulation Setup

Our integrated MATLAB-hardware simulation flow shown in Fig. 1 allows us to seamlessly switch between a 60 GHz hardware testbed and statistically generated impairments and channel models. The testbed setup is based on commercially available laboratory grade Sivers IMA FC1005V 60 GHz analog front-ends. A Tektronix AWG7122C arbitrary waveform generator is used as a signal source, and an R&S RTO1044 oscilloscope acquires the received waveform. An Agilent E5052A signal source analyzer was used to directly measure the PN. The setup supports channel bandwidths of up to 3 GHz and frame lengths up to 5 ms. This hardware radio link serves as a reference for our analysis. It is used to extract and validate the parameters for the channel and phase noise simulations. EVM performance figures are then obtained by means of Monte-Carlo simulations. All simulations in this paper are based on transmission parameters and a frame structure derived from the IEEE 802.11ad standard [3]. A symbol rate of 1.76 GSPS and a code word length $N_{\mathrm{CW}} = 672$ is used. We further assure in our setup a perfect initial synchronization.

The measurement results shown in Fig. 2 suggest a PN performance of our 60 GHz front-ends which is more than 10 dB worse than a commonly used ADI AD4350 PLL at the 2.4 GHz ISM band. A literature survey reveals that the gap between 60 GHz PLLs and 2.4 GHz PLLs increases even further if we compare against power-efficient 60 GHz PLL designs [4][5][6] based on a standard CMOS process.

B. Performance

The distortion of the received vectors by PN worsens over time. Hence, the presence of PN is especially severe for

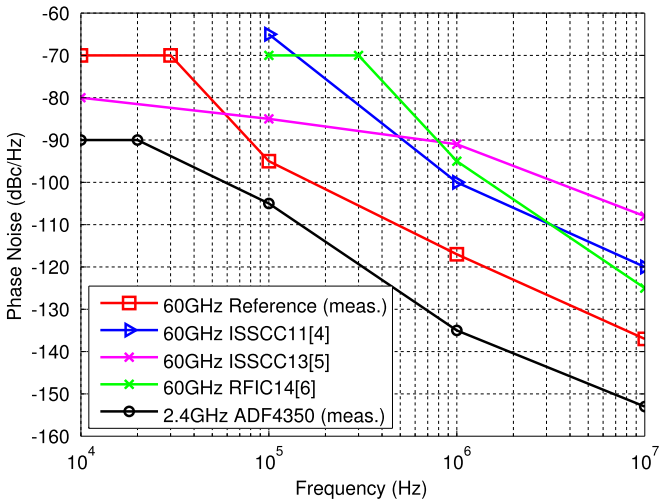

Fig. 2. Comparison of phase noise between our reference 60 GHz PLL, a commercial 2.4 GHz PLL, and various reported academic 60 GHz PLL designs.

applications, relying on long frames. For example the high-throughput video streaming applications described above are based on long frames to reduce transmission overhead and maximize link efficiency. For the IEEE802.11ad standard the maximum time for a frame is 2ms. Our measurements show that already for significantly shorter frame lengths fatal error situations are induced and that PN compensation is mandatory.

As the influence of PN can strongly vary during the transmission of a frame, the EVM value e_i is calculated as a function of the position i within the frame. It is assumed a certain level of distortion is only critical if it persists for a period longer than what could be fixed by an error correction code. Hence channel coding is taken into account by calculating e_i (4) over an averaged window. The windows size $N_{\mathrm{WS}} = \frac{N_{\mathrm{CW}}}{M}$ was chosen to be the length of a code word N_{CW} divided by the modulation order M.

$$e_i = \sqrt{\frac{1}{N_{\mathrm{WS}}} \sum_{u=i}^{i+N_{\mathrm{WS}}-1} \left(r_u - \sum_{k=0}^{N_{\mathrm{CIR}}-1} s_u h_{u-k} \right)^2} \quad (4)$$

$$e_i^{\mathrm{wc}} = \max_{u=0,..,i} (e_u) \quad (5)$$

Based on the high level assumption that a frame that has at some point faced fatal distortion needs to be discarded completely we are interested in the worst-case value of e_i. Hence e_i^{wc} is found by taking the maximum value according to (5) up to time i.

Fig. 3 shows the expectation of e_i^{wc} due to the influence of PN in a thermal-noise free environment as a function of the time. The maximal acceptable EVM for different modulation schemes with coding are marked by horizontal lines. The values are taken from a link budget analysis for wide band 60 GHz communication in [7]. Therefore the figure indicates the maximal usable frame length for a certain modulation without PN compensation. We see that even for BPSK modulation that frame length beyond 400 us are not feasible.

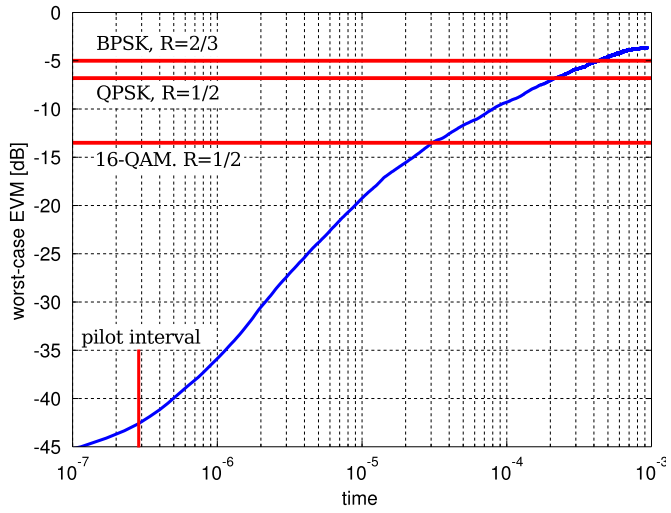

Fig. 3. The expectation of the worst-case EVM e^{wc} of the received signal under the influence of PN as a function of the length of the frame.

The simulation results also confirm our assumption that PN can be considered constant for the duration of the delay spread as the introduced error is way below -45 dB EVM.

III. Low-Complexity Auto-Correlation Based Estimator

Decision-directed PN estimation approaches have been proposed for 60 GHz systems [8][9] as they are a convenient extension of receivers based on linear equalizers. However these schemes suffer not only from the effect of error propagation in low SNR regimes, but also put a delay constraint on the receiver chain.

An iterative method to achieve improved performance and reduce the impact of error-propagation is presented in [10]. Such a strategy can result in good performance but comes at the cost of a multiplication of complexity and latency. A general problem of decision-directed schemes is the integration into receivers which do not calculate equalized symbols.

To adress these problems we propose an alternative PN estimation scheme based on data-aided auto-correlation, which exploits the existing frame structure of the IEEE802.11ad standard.

A. Algorithm

As shown in Fig. 4, the data is split into chunks, which are prepended with a pilot word of length $N_{\text{GI}} = 64$. The pilot words act as guard intervals (GI), resulting in blocks of length N_{BLK}. Such pilot words are mandatory in the IEEE802.11ad standard to improve equalization, and form a recurring field of data in the transmitted frame. The samples, $p_{k,i} = r_{(k \cdot N_{\text{BLK}})+i}, i = 0, .., N_{\text{GI}}\text{-}1$ correspond to the pilot of the kth block. Assuming that the observed delay spread is shorter than the length of the pilot word and the channel conditions are static during the transmission, the received samples contain a periodically field which differs in phase and

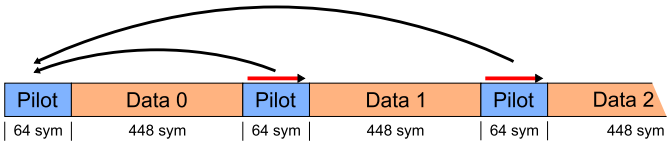

Fig. 4. Data blocks of the assumed frame format, interleaved with pilot words. Correlation is always performed with the first pilot word.

thermal noise only. Measurements with our hardware testbed confirm that the channel can be considered static during one transmission and PN is the dominant distortion.

According to (1) PN manifests itself in a rotation of the phase of the received symbols. The first pilot field can be used as a reference. Multiplying a symbol of a pilot word at time i with the complex conjugate of the corresponding symbol of the reference pilot word gives an estimate of the PN. Unfortunately, the received pilot words are distorted by thermal noise, which can lead to an additional phase deviation. From Fig. 3 we know that we can consider the phase noise as constant for the duration of a pilot field. Performing the correlation over multiple symbols of the pilot word leads to a processing gain and reduces the influence of thermal noise. The length, L_{corr}, of the usable correlation window is dependent on the observed delay spread, and defines the degree of available noise suppression. L_{corr} amounts to the number of symbols of the GI which are not influenced by ISI from a previous data block

$$L_{\text{corr}} = N_{\text{GI}} - N_{\text{CIR}} + 1. \tag{6}$$

The estimation of the phase offset, $\hat{\phi}_k$, of the kth block can be calculated as

$$\hat{\phi}_k = arg\left(\sum_{i=N_{\text{CIR}}}^{N_{\text{GI}}-1} p_{k,i} p_{0,i}^{*}\right). \tag{7}$$

Due to the short interval between pilot sequences, it is sufficient to perform the estimation at the block rate $R_B = 3.43$MHz and still capture the significant part of the PN energy.

Fig. 5 shows the performance of our proposed PN compensation scheme under different SNR regimes in comparison to an uncorrected transmission and a scenario without any phase noise. The auto-correlation based compensation can cancel nearly the complete PN. The error of the residual PN accounts for a degredation of less then 0.3 dB.

As stated earlier delay spread limits the available processing gain for the PN estimation. Fortunately, N_{GI} is substantially longer than the expected delay spread given for many published 60 GHz equalization architectures [11][8][12] which can equalize a delay spread between 2 and 8 taps. Fig. 6 and Fig. 7 show how our PN compensation performs as a function of the correlation length for 10 dB and 20 dB SNR. The results show that for $L_{\text{corr}} > 32$ the loss compared to the full correlation length is below 0.4 dB. Hence the algorithm exhibits very good performance even for a delay spread of more than 30 taps.

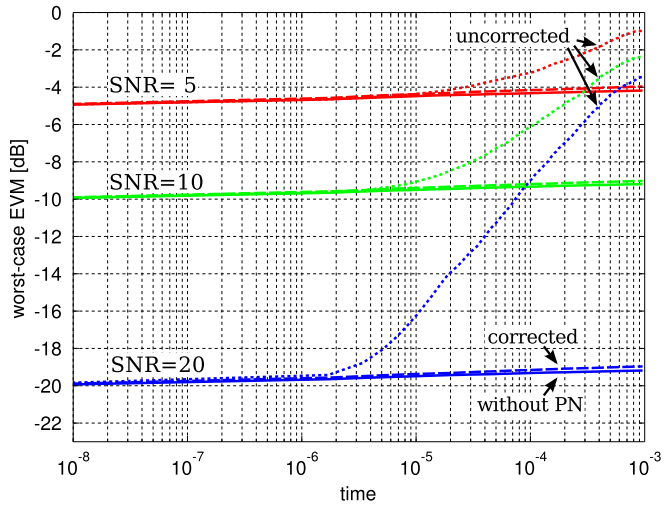

Fig. 5. Worst-case EVM before and after low complexity PN compensation for different SNR. The phase-noise free case marks the lower bound for the performance.

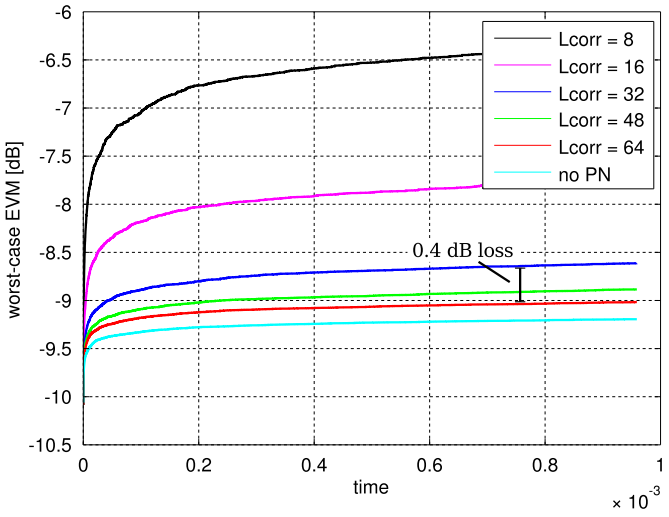

Fig. 6. Performance of the low complexity PN compensation for different correlation lengths L_{corr} at 10dB SNR.

IV. Implementation Considerations

The absence of feedback paths from other subsystems of the baseband receiver leads to a very regular and self-contained architecture for our proposed algorithm, as can be seen in Fig. 8. Our architecture is flexible for system integration as it is agnostic to the used equalization and detection scheme. The windowed auto-correlation operation allows a variable degree of parallelism. As a result it adapts well to different system-level strategies, because not only compact high-speed VLSI implementations but also highly-parallelized versions for FPGA environments are possible.

Compensating with the last known phase-noise before estimating residual PN, allows the direct output of

$$\Delta\hat{\phi}_n = \hat{\phi}_n - \hat{\phi}_{n-1}, \tag{8}$$

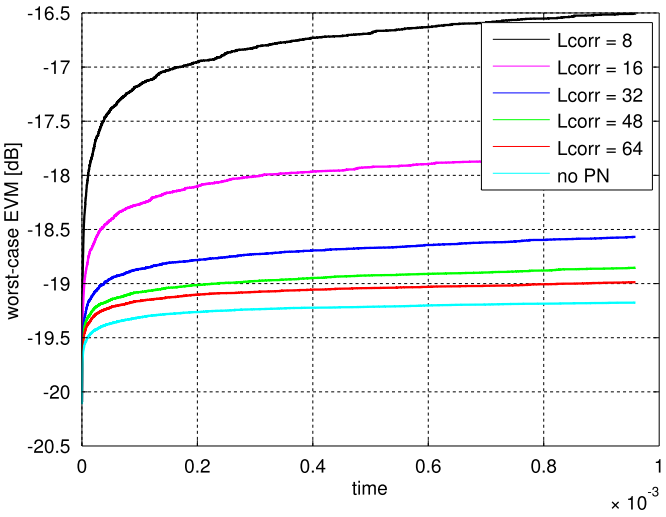

Fig. 7. Performance of the low complexity PN compensation for different correlation lengths L_{corr} at 20dB SNR.

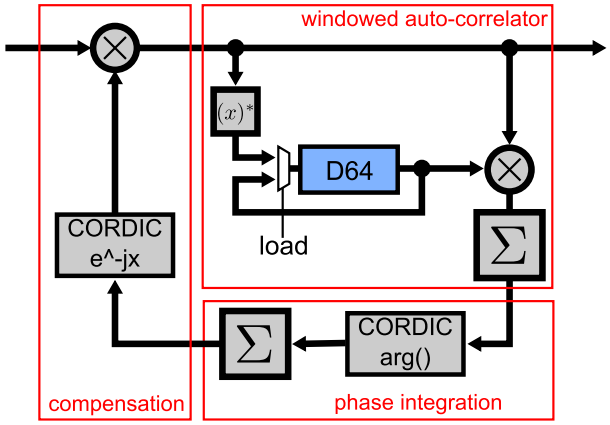

Fig. 8. Proposed self-contained architecture for phase noise estimation and compensation.

which can be used after low-pass filtering to detect any residual frequency offset. Such information can be used for improved sampling frequency offset (SFO) correction and better timing interpolation. The large resemblance of the proposed PN estimation architecture to the well known Schmidl&Cox [13] frequency synchronization algorithm allows for many practical receivers to share large parts of the circuitry with the synchronization unit and further reduces the costs of the implementation.

V. Conclusion

We have shown that phase noise severely limits the maximal frame lengths for 60 GHz. Frame length longer than 400 us are not feasible even for BPSK and hence compensation is crucial to obtain high link efficiency in 60 GHz systems. Our presented auto-correlation based algorithm provides excellent noise surpression up to 30 taps of delay spread. An efficient hardware implementation exists which is well suited for easy integration in different scenarios.

REFERENCES

[1] T. S. Rappaport, S. Sun, R. Mayzus, H. Zhao, Y. Azar, K. Wang, G. N. Wong, J. K. Schulz, M. Samimi, and F. Gutierrez, "Millimeter wave mobile communications for 5G cellular: It will work!" *Access, IEEE*, vol. 1, pp. 335–349, 2013.

[2] Y. Zhu, Z. Zhang, Z. Marzi, C. Nelson, U. Madhow, B. Y. Zhao, and H. Zheng, "Demystifying 60GHz outdoor picocells," 2014.

[3] "IEEE standard for information technology–telecommunications and information exchange between systems–local and metropolitan area networks–specific requirements-part 11: Wireless LAN medium access control (MAC) and physical layer (PHY) specifications amendment 3: Enhancements for very high throughput in the 60 GHz band," *IEEE Std 802.11ad-2012 (Amendment to IEEE Std 802.11-2012, as amended by IEEE Std 802.11ae-2012 and IEEE Std 802.11aa-2012)*, pp. 1–628, Dec 2012.

[4] U. Decanis, A. Ghilioni, E. Monaco, A. Mazzanti, and F. Svelto, "A mm-wave quadrature VCO based on magnetically coupled resonators," in *Solid-State Circuits Conference Digest of Technical Papers (ISSCC), 2011 IEEE International*. IEEE, 2011, pp. 280–282.

[5] X. Yi, C. C. Boon, H. Liu, J. F. Lin, J. C. Ong, and W. M. Lim, "A 57.9-to-68.3 ghz 24.6 mw frequency synthesizer with in-phase injection-coupled QVCO in 65nm CMOS," in *Solid-State Circuits Conference Digest of Technical Papers (ISSCC), 2013 IEEE International*. IEEE, 2013, pp. 354–355.

[6] T. Siriburanon, T. Ueno, K. Kimura, S. Kondo, W. Deng, K. Okada, and A. Matsuzawa, "A 60-GHz sub-sampling frequency synthesizer using sub-harmonic injection-locked quadrature oscillators," in *Radio Frequency Integrated Circuits Symposium, 2014 IEEE*, June 2014, pp. 105–108.

[7] S. Krone, F. Guderian, G. Fettweis, M. Petri, M. Piz, M. Marinkovic, M. Peter, R. Felbecker, and W. Keusgen, "Physical layer design, link budget analysis, and digital baseband implementation for 60 GHz short-range applications," *International Journal of Microwave and Wireless Technologies*, vol. 3, pp. 189–200, 3 2011.

[8] W.-C. Liu, F.-C. Yeh, T.-C. Wei, C.-D. Chan, and S.-J. Jou, "A digital Golay-MPIC time domain equalizer for SC/OFDM dual-modes at 60 GHz band," *Circuits and Systems I: Regular Papers, IEEE Transactions on*, vol. 60, no. 10, pp. 2730–2739, 2013.

[9] K. M. et al., "An integrated 60GHz low power two-chip wireless system based on IEEE802.11ad standard," in *Microwave Symposium (IMS), 2014 IEEE MTT-S International*, June 2014, pp. 1–4.

[10] S. Suyama, Y. Miyai, H. Suzuki, and K. Fukawa, "Experimental evaluation of phase noise compensation for 60-GHz single carrier systems," in *Wireless Technology Conference (EuWIT), 2010 European*. IEEE, 2010, pp. 289–292.

[11] C. Marcu, D. Chowdhury, C. Thakkar, L.-K. Kong, M. Tabesh, J.-D. Park, Y. Wang, B. Afshar, A. Gupta, A. Arbabian, S. Gambini, R. Zamani, A. M. Niknejad, and E. Alon, "A 90nm CMOS low-power 60GHz transceiver with integrated baseband circuitry," in *Proc. IEEE Int. Solid-State Circuits Conf. - Digest of Technical Papers ISSCC 2009*, 2009, pp. 314–315.

[12] K. Okada, K. Kondou, M. Miyahara, M. Shinagawa, H. Asada, R. Minami, T. Yamaguchi, A. Musa, Y. Tsukui, Y. Asakura, S. Tamonoki, H. Yamagishi, Y. Hino, T. Sato, H. Sakaguchi, N. Shimasaki, T. Ito, Y. Takeuchi, N. Li, Q. Bu, R. Murakami, K. Bunsen, K. Matsushita, M. Noda, and A. Matsuzawa, "Full four-channel 6.3-Gb/s 60-GHz CMOS transceiver with low-power analog and digital baseband circuitry," *Solid-State Circuits, IEEE Journal of*, vol. 48, no. 1, pp. 46 –65, jan. 2013.

[13] T. M. Schmidl and D. C. Cox, "Robust frequency and timing synchronization for OFDM," *Communications, IEEE Transactions on*, vol. 45, no. 12, pp. 1613–1621, 1997.